ISSN 1068-798X, Russian Engineering Research, 2017, Vol. 37, No. 11, pp. 962–968. © Allerton Press, Inc., 2017.
Original Russian Text © Yu.G. Kabaldin, A.A. Kuz'mishina, V.O. Zotov, E.E. Vlasov, 2017, published in Vestnik Mashinostroeniya, 2017, No. 8, pp. 75–81.

Influence of Cut Layer on Cutting

Yu. G. Kabaldin*, A. A. Kuz'mishina, V. O. Zotov, and E. E. Vlasov

Alekseev Nizhny Novgorod State Technical University, Nizhny Novgorod, Russia

**e-mail: uru.40@mail.ru*

Abstract—The contact of the chip with the tool's front surface in cutting is analyzed by numerical modeling. The high-pressure zones and buildup at the tool's contact surface are studied. The influence of plastic instability of the chip surface and vortex deformation modes on tool wear is considered.

Keywords: cutting, chip, tools, vortex deformation modes, high-pressure zones, buildup, wear

DOI: 10.3103/S1068798X17110053

Experiments show that, in cutting, complex processes develop in the chip and in the contact layers of the tool. In particular, vortical flow of the particles is observed [1]. We may better understand the wear of the hard-alloy tool if we study the loss of plastic stability in contact layers of the workpiece.

STRESS–STRAIN STATE OF THE TOOL AND WORKPIECE IN CUTTING

By numerical modeling of the stress–strain state in the tool and workpiece (Fig. 1), we find that, in the zone of the chip closest to the cutter, the compressive stress σ_{22} is converted to tensile stress [2, 3]. Close to the cutter, the chip is not in contact with the tool's front surface. The primary contact is observed at a distance of 0.26 mm from the cutter, where the compressive normal stress is 300–450 MPa. There is a small contact spot. In other words, we observe discontinuous contact of the chip with the tool's front surface, where friction is present.

In Fig. 2, the band seen in the vicinity of the cutting edge confirms the theoretical conclusion that there is no contact of the chip particles with the tool close to the cutter.

The primary retardation of the chip layers at the cutter in the machining of steel 45 (Fig. 3) confirms

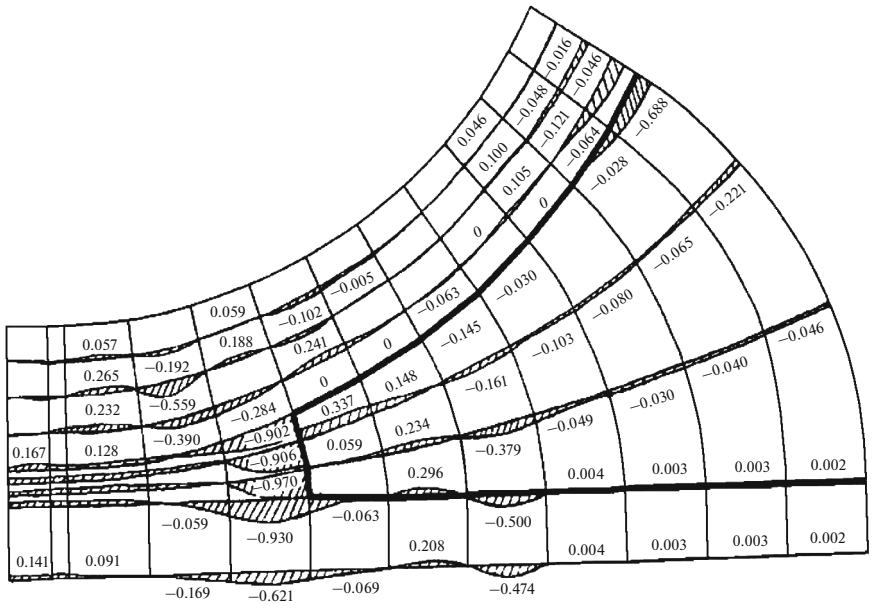

Fig. 1. Stress–strain state in the cutting zone.

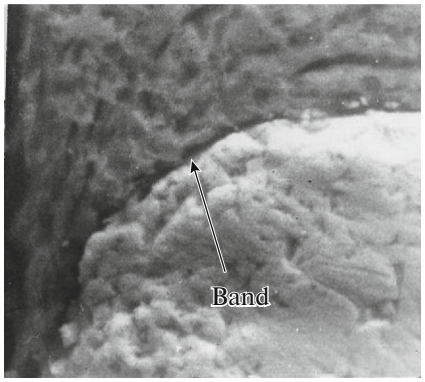

Fig. 2. Band in the vicinity of a VK8 alloy cutter in the case of a steel 45 workpiece (×5000): $v = 1$ m/s; $a = 0.2$ mm.

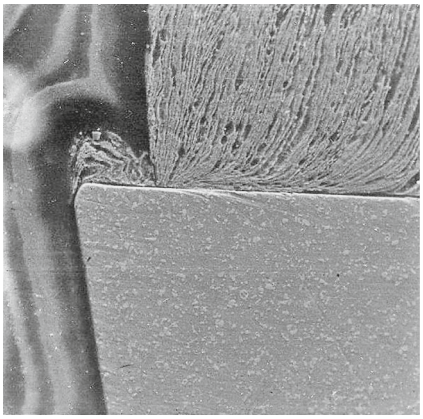

Fig. 3. Tight contact of the chip and the tool's front surface, with the formation of texture at some distance from the cutting edge (×1000).

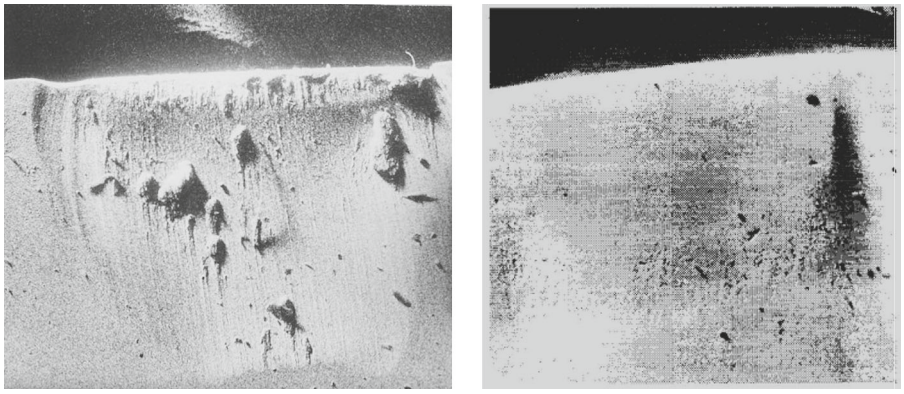

Fig. 4. Interaction of chip with a VK8 alloy tool (×1000): (a) metal particles welded after shear of the buildup over the front surface; (b) craters and edge wear of the front cutter surface after etching of the metal particles.

the formation of texture with buildup at some distance from the cutting edge.

Welded particles of the workpiece are seen at the tool's front surface (Fig. 4). That indicates intense adhesion. It is clear from the distribution of workpiece particles (Fig. 4a) and the initial wear of the contact areas (Fig. 4b) that the adhesion and wear are most intense at some distance from the cutting edge. At the end of chip–tool contact, which is characterized by friction of the oxidized surfaces, the adhesive processes are reduced. The same results are obtained in calculating the stress–strain state of the contacting surfaces in cutting (Fig. 1).

The two-zone model of chip–tool contact is widely adopted at present (Fig. 5a): (1) plastic contact C_{pl}; (2) an external zone characterized by friction or discontinuous contact (C_{ex}) [1].

We find that plastic contact includes different stages. The first stage is a discrete process: retarded primary-contact regions are formed and experience high compressive stress. The second stage is the development of plastic contact, with the appearance of buildup (a tapered body that acts as a cutter). In section C_d (Fig. 5b), we observe deformational (cohesive) buildup, without adhesion. This is confirmed by experimental data (Fig. 4): close to the cutting edge, there is no adhesion, and the buildup is laminar.

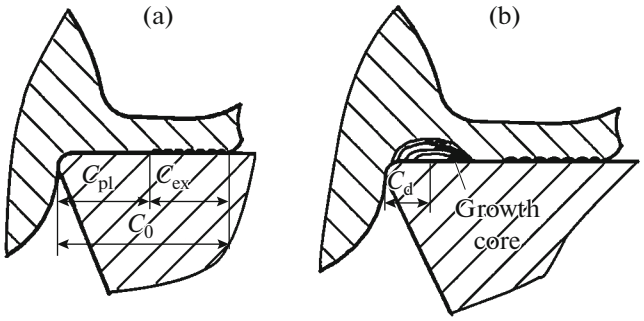

Fig. 5. Existing (a) and proposed (b) two-zone models of contact between the chip and the tool's front surface.

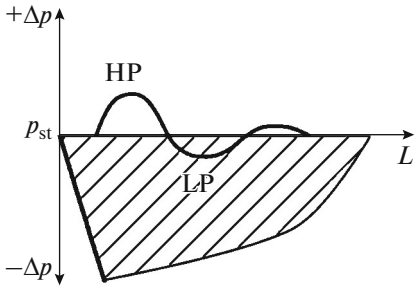

Fig. 6. Zones of high pressure (HP) and low pressure (LP) at the tool's front surface.

In cutting, regions of high and low pressure appear (Fig. 6). The high-pressure regions at the tool's front surface (length L) and rear surface determine the tool buildup and wear.

In Fig. 7a, we show part of the buildup formed in cutting steel 10. After shear of the buildup relative to the tool's front surface, a vortex structure is formed. That indicates considerable strain ε of the layers at the cutter, in view of the large normal stress σ_N at the tool's working surface and the stability loss of the workpiece.

X-ray microspectral analysis of sections of VK8 alloy plates and the buildup in the boundary layer reveals increased Si and Mn content.

PLASTIC INSTABILITY IN THE WORKPIECE AT THE CUTTER

The vortical motion of the workpiece particles (Fig. 7) indicates considerable deformation of the layers near the cutter. With deformation and the accumulation of dislocations in local volumes, the crystal lattice of the material is distorted. The limiting lattice distortion corresponds to the critical dislocation density ρ_{cr} in local volumes of the metal. We assume that the unit deformational energy ΔU_d is consumed in the limiting lattice distortion and rupture of the interatomic bonds. Then we may write

$$\Delta U_d = E_0 \rho_{cr}, \quad (1)$$

where E_0 is the dislocational energy per unit length.

Calculations show that the metal lattice is disrupted, and it is close to amorphous when $\rho_{cr} = 10 \times 14$ cm^{-2} [4].

Electron-diffraction data confirm that the crystal lattice becomes amorphous in deformed local volumes, both in the contact layer of the chip and in the buildup (Fig. 8).

Thus, in steady cutting, melting of the deformed workpiece volumes and vortical motion of the particles may be observed in the chip close to the cutter (Fig. 1).

In the first approximation, the temperature rise in the chip close to the cutter on contact with the tool's front surface is $\Delta T = \tau_s \varepsilon / C_V$, where τ_s is the slipping stress and C_V is the specific heat.

For steel, $\tau_s = 5 \times 10^5$ N/m^2; $C_V = 5000$ J/(m^3 K); and $\varepsilon = 30$. In that case, $\Delta T = 1400$ K, which is close to the melting point of U8 steel, for example. Experimental data show that the dislocation density ρ may be about 10^{12}–10^{14} cm^{-2} in local volumes [1, 2]. That indicates lattice failure in the intensely deformed metal volumes.

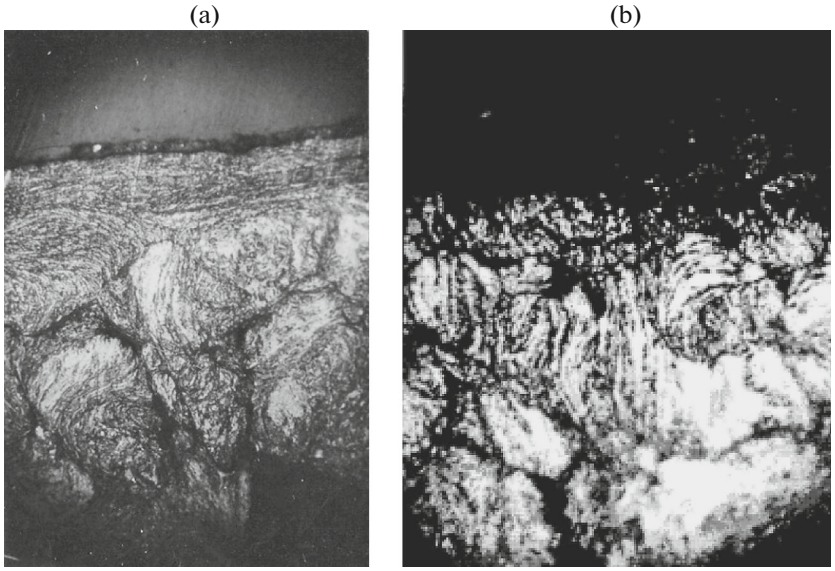

Fig. 7. Slowing of workpiece particles at the tool's front surface in the machining of steel 10 with $v = 15$ (a) and 35 m/min (b) (×200).

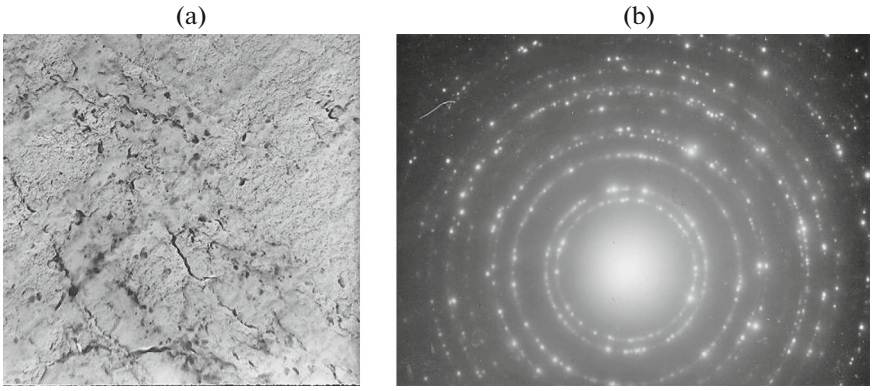

Fig. 8. Amorphous structure of the steel 10 layer close to the cutter: (a) buildup (×3000); (b) electron-diffraction pattern from the given layer.

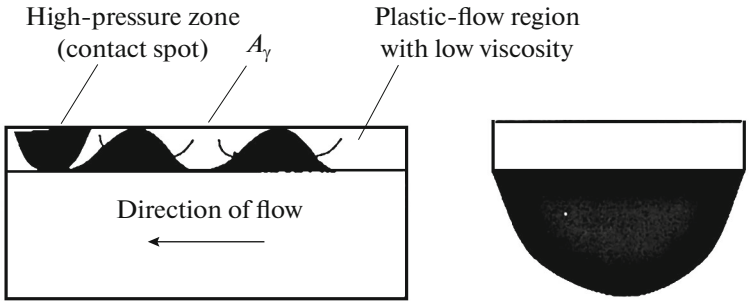

Fig. 9. Chip motion relative to a high-pressure zone and soliton generation.

Thin-foil data for the dislocation structure also show that the dislocation density is critical in the chip close to the cutter within high-pressure zones [5].

On the basis of the quasi-liquid state of the chip layers close to the cutter, we may assume that buildup forms as a result of the motion of unit waves toward the cutter, analogously to a soliton (Fig. 5b). Mathematical models and methods of numerical modeling of soliton generation were presented in [5, 6]. The motion of high-pressure zones over the surface of a liquid bounded by impermeable walls is considered.

Localized high-pressure zones in the layer close to the cutter nay be primary sources of retardation of the machined material—that is, sources of adhesion.

In Fig. 9, we show chip motion relative to a high-pressure zone and soliton generation. The front surface of the cutter is at the top. The solitons may be formed from the chip and from the tool. A trough is formed behind the soliton.

We now consider the appearance of individual vortices in the viscoplastic contact layers, on the basis of [5, 6]. We employ the generalized Boussinesq approximation. The functions to be determined are the profile $\eta(x, t)$ of plastic tool–workpiece contact; and the mean tangential velocity component $u(x, t)$ over the plastic contact width. The evolution of these functions is described by the following equations

$$\left.\begin{aligned} \eta_t + [(1+\eta)u]_x = 0; \\ u_t + uu_x + \eta_x + p_x = 1/3u_{txx}, \end{aligned}\right\} \quad (2)$$

where $P(x, t)$ is the pressure distribution at contact. The subscripts denote partial differentiation with respect to the corresponding variables.

In Fig. 10, we show the formation of buildup and plasticity waves at the tool's front surface and the formation of local adhesion. Over the contact length, we observe moving low- and high-pressure zones. Hence, the pressure $p(x, t)$ in Eq. (3) is nonuniform, in contrast to the solution in [5].

Now consider the flow of material in cutting with a single high-pressure zone, which moves over the plastic layer. According to Fig. 1, we may assume that $p = 0$ at the edge of this region, while $p = p_m \neq 0$ at its center. Therefore, we may specify the high-pressure zone in the form

$$p(x,t) = p(\xi) = \begin{cases} pm\cos^2\left(\dfrac{\pi\xi}{2}\right) & \text{when } |\xi| \le 1; \\ 0 & \text{when } |\xi| > 1, \end{cases} \quad (3)$$

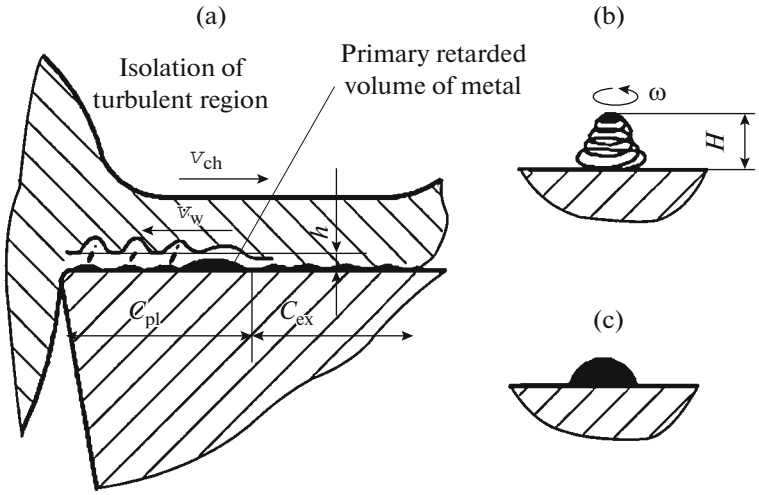

Fig. 10. Formation of buildup and plasticity waves at the tool's front (a) surface and the formation of local adhesion (b, c).

where $\xi = (x - vt)/l$ is the local coordinate in the reference system corresponding to the tool; v is the cutting speed; l is the size of the high-pressure zone.

Thus, in the layer close to the cutter, the high-pressure zone is characterized by velocity $v = \text{const}$, the dimension l, and the pressure $p_m = p_0(0)$. The initial data adopted are the initial contact profile $\eta_0(x)$ and the initial velocity $u_0(x)$

$$\left.\begin{aligned} \eta &= \eta_0(x); \\ u &= u_0(x) \text{ when } t = 0. \end{aligned}\right\} \tag{4}$$

Numerical solution of the differential equations is based on the finite-difference method. Discretization with respect to the time is based on the implicit Crank–Nicholson scheme. For convenience in constructing the difference grid, we write the system of equations in the form

$$\begin{cases} \eta_t + q_x = 0; \\ \omega_t + s_x = 0, \end{cases} \tag{5}$$

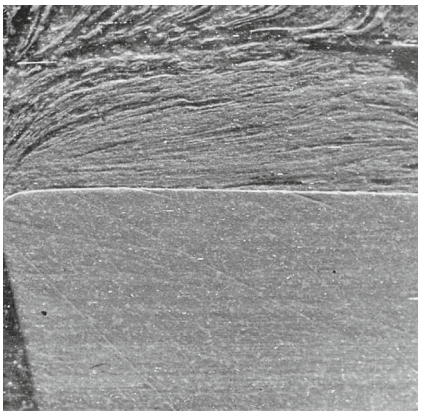

Fig. 11. Buildup consisting of deformed metal layers.

where

$$\begin{aligned} q(x,t) &= (1+\eta)u; \\ \omega(x,t) &= u - (1/3)u_{xx}; \\ s(x,t) &= (1/2)u^2 + \eta + p. \end{aligned} \tag{6}$$

We assume that the liquid–plastic layer in the chip is initially at rest

$$\begin{aligned} \eta_0(x) &= -p(x,0); \\ \omega_0(x) &= 0 (\Leftarrow u_0(x) = 0). \end{aligned} \tag{7}$$

For the calculation, we need to define the range of x: $-l_1 \le x \le l_2$. In the first approximation, we assume that the liquid–plastic layer is in a channel with impermeable boundaries. Then

$$\left.\begin{aligned} u &= 0 \text{ when } x = -l_1 \text{ and } x = l_2; \\ q &= 0 \text{ when } x = -l_1 \text{ and } x = l_2. \end{aligned}\right\} \tag{8}$$

The difference system of equations takes the form

$$\begin{cases} \eta^{n+1,k+1} + \dfrac{\Delta t}{2} q_x^{n+1,k} = \eta^n - \dfrac{\Delta t}{2} q_x^n; \\ \omega^{n+1,k+1} + \dfrac{\Delta t}{2} s_x^{n+1,k} = \omega^n - \dfrac{\Delta t}{2} s_x^n, \end{cases} \tag{9}$$

where Δt is the increment; the first superscript corresponds to the number of the time step, and the second to the number of the iteration.

Solution of Eqs. (2)–(9) indicates that a high-pressure zone moving over the surface of a plastic layer may periodically generate waves of soliton type moving over the flux toward the cutter tip (Fig. 11). The solitons appear at some critical cutting speed u_{cr}. With increase in pressure p_m, the frequency of soliton generation increases, along with their amplitude and velocity. As a result of the consumption of the plastic material in soliton generation, a trough appears behind the

high-pressure zone in the layer close to the cutter. With increase in cutting speed, the frequency of soliton generation decreases; with increase in the chip's plastic-layer thickness, the frequency of soliton generation increases.

We now determine the relaxation time and energy of the deformational solitons. Calculations indicate that the relaxation time of the deformational solitons is around 10^{-2}–10^{-5} s.

In the first approximation, the soliton energy is $\Delta E = F_d v_s$, where F_d is the force on unit length of the soliton and v_s is the soliton velocity (close to the speed of sound).

The velocity and energy of the deformational solitons depend on the medium. Thus, in the present case, they depend on the material being deformed. In some materials, the dislocational velocity v_d is close to the speed of sound. It is higher in metals with an fcc lattice than in bcc metals. The velocity v_d also depends on the packing-defect energy of the metal.

The soliton energy exceeds the unit destructive energy ΔE_{un} of the binder and carbide grains in hard alloys.

The thermal power of a solid with dislocation density ρ is $Q_0 = 10^8 \rho^{1/3} \varepsilon q_0$ [7]. Here ε is the strain in the local high-pressure zones; q_0 is the thermal power of a single dislocation.

The temperature in the local volumes is found from the formula $\theta = Aq_0\sqrt{\tau_s}$, where τ_s is the soliton lifetime.

Calculations show that, with considerable soliton life ($\tau_s = 10^{-5}$ s), the temperature θ is established practically instantaneously and exceeds the melting point of most machined materials.

In Fig. 10, we illustrate the formation of buildup and plasticity waves at the tool's front surface and the formation of local adhesion. The notation is as follows: h, thickness of the quasi-liquid chip layer close to the cutter; H, height of the vortical column; ω, angular velocity of the vortex; v_{ch}, chip velocity; v_w, wave velocity.

The solitons generated by the high-pressure zones are the nuclei of new dynamic dissipative flow structure in the layer close to the cutter. In the cut layer, at the cutter tip, three-dimensional perturbations of relatively large amplitude are concentrated. These may be converted to turbulence as a result of nonlinear processes.

In cutting, the plastic flow of the contact layers leads to stability loss of the material and the creation of individual turbulent zones immersed in the laminar flow (Fig. 10a). Hence, the buildup is an individual stationary turbulent zone at the cutter tip, where layers of the material are mixed. Thus, local mass-transfer

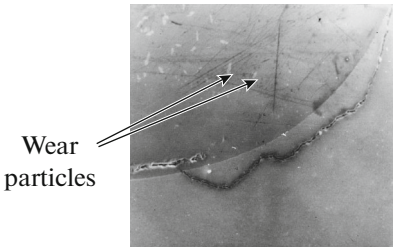

Fig. 12. Transverse section with the front surface of a T15K6 alloy tool, in which a crater is filled with titanium-alloy wear particles and tool particles (white particles in the top left).

zones are formed by a vortical (rotary) mechanism and remain at the tool's front surface in the form of buildup. This may be attributed, on the one hand, to the increase in pressure associated with solution motion over a liquid surface; and, on the other, to interaction of the liquid layers with surface layers of the tool, subsequent adhesion, and blocking of the flow.

Thus, we observe rotary deformation modes (Fig. 10b), and a vortical column is formed. Its height is determined by the thickness of each layer, the properties of the machined material, and the flow velocity of the liquid. The latter factors affect the strengthening of the buildup. The buildup height increases after the formation of the core under the action of individual waves at the surface of the liquid layer, moving toward the cutter. Therefore, the buildup has a laminar structure; it consists of deformable layers (Fig. 11).

The formation of buildup under the action of waves on a quasi-liquid layer is confirmed in that the crystalline structure of the buildup cannot be discerned by metallographic methods (Fig. 8a). In other words, the metal in the buildup is also in an amorphous–crystalline state.

Solitons are mainly formed from the workpiece material. If nuclei of vortical structure are formed from the surface layer of the cutter, tool particles are entrained from the high-pressure zones. In other words, wear occurs.

In Fig. 12, we show a section of a T15K6 alloy tool after machining titanium alloy. In Fig. 13, the vortical motion of wear particles from the tool in a crater at the front surface of T15K6 alloy is shown. In the crater and in the workpiece material that fills it, white spots are seen. These are particles torn from the tool. This distribution of tool particles is only possible in the case of a liquid state and vortical motion in the workpiece, with mixing of the layers. In Fig. 13b, the wear particles are above the tool's contact surface.

The wear particles from the tool move over its front surface (Fig. 13a) and then, as a result of vortical motion, particles in the workpiece layers close to the cutter move into the chip (Fig. 13b). Particle rupture

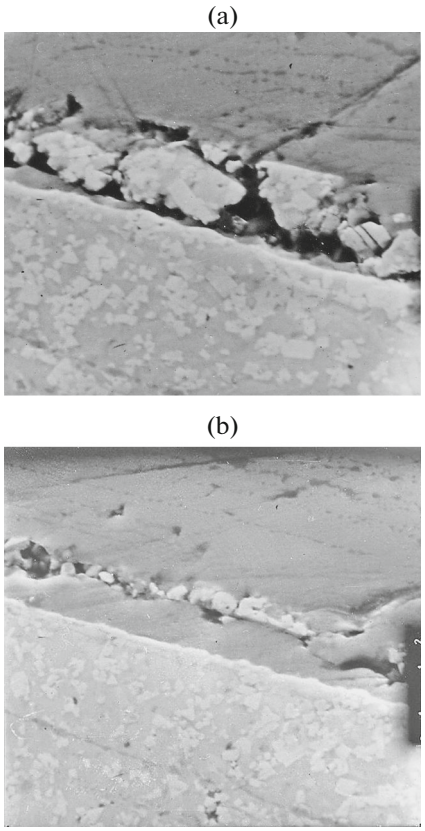

Fig. 13. Vortical motion of wear particles from the tool in a crater at the front surface of T15K6 alloy (×1500).

occurs as a result of fatigue processes or local fracture of the tool associated with strong adhesion to the workpiece.

On the basis of theoretical and experimental data, we have established that wear of the hard-alloy tool is a vortical process. On that basis, we have developed means of improving the wear resistance of tools.

REFERENCES

1. Zorev, N.N., *Voprosy mekhaniki protsessa rezaniya* (Mechanics of Cutting Process), Moscow: Mashgiz, 1956.
2. Kabaldin, Yu.G., Shpilev, A.M., and Burkov, A.A., Soliton mechanism of vibration perturbation in technological self-organizing systems, *Vestn. Mashinostr.*, 2000, no. 3, pp. 31–37.
3. Kabaldin, Yu.G., Oleinikov, A.I., and Burkov, A.A., Synergetics of the evolution of structures and soliton mechanisms of friction, wear, and lubrication during cutting, *Vestn. Mashinostr.*, 2000, no. 1, pp. 34–41.
4. Pavlov, V.A., Amorphization of the structure of metals and alloys with an extremely high degree of deformation, *Fiz. Met. Metalloved.*, 1985, vol. 59, no. 4, pp. 629–649.
5. Belotserkovskii, O.M., *Chislennyi eksperiment v turbulentnosti: ot poryadka k khaosu* (Numerical Experiment in Turbulence: From Order to Chaos), Moscow: Nauka, 1997.
6. Chernyi, G.G., The motion of a melting solid between two semispaces, *Dokl. Akad. Nauk SSSR*, 1985, vol. 282, no. 4, pp. 814–818.
7. Krasulin, Yu.P. and Timofeev, V.N., Heat release on contact surfaces during metal processing, in *Fiziko-mekhanicheskie i teplofizicheskie svoistva metallov* (Physical-Mechanical and Thermophysical Properties of Metals), Moscow: Nauka, 1976, pp. 132–136.
8. Panin, V.E., Likhachev, V.A., and Grinyaev, Yu.V., *Strukturnye urovnii deformatsii tverdykh tel* (Structural Levels of Deformation in Solids), Novosibirsk: Nauka, 1985.
9. Kabaldin, Yu.G., Seryi, S.V., Kretinin, O.V., et al., *Komp'yuternoe modelirovanie i issledovanie nanostruktur v protsessakh obrabotki rezaniem na osnove kvantovomekhanicheskikh raschetov* (Computer Modeling and Study of Nanostructures in the Cutting Processes Based on Quantum Mechanical Calculations), Nizhny Novgorod: Nizhegorod. Gos. Tekh. Univ., 2014.

Translated by Bernard Gilbert